Energy & Environmental Science

GaSb Doping Facilitates Conduction Band Convergence and Improves Thermoelectric Performance in n-type PbS

Journal:	*Energy & Environmental Science*
Manuscript ID	EE-ART-01-2023-000183.R1
Article Type:	Paper
Date Submitted by the Author:	09-Feb-2023
Complete List of Authors:	Chen, Zixuan; Fuzhou University, College of Materials Science and Engineering Cui, Hong-Hua; Fuzhou University, Mechanical and Electrical Engineering Practice Center Hao, Shiqiang; Northwestern University, Materials Science Liu, Yukun; Northwestern University, Department of Materials Science and Engineering Liu, Hui; University of Science and Technology Beijing, Zhou, Jing; Fuzhou University, College of Materials Science and Engineering Yu, Yan; Fuzhou University Yan, Qingyu; Nanyang Technological University, MSE Wolverton, Chris; Northwestern University, Department of Materials Science and Engineering Dravid, Vinayak; Northwestern University, Materials Science & Engineering Luo, Zhong-Zhen; Fuzhou University, College of Materials Science and Engineering Zou, Zhigang; Nanjing University, Physics Kanatzidis, Mercouri; Northwestern University, Department of Chemistry

Thermoelectric technology, with the advantages of small size, no moving parts, long steady-state operation periods, and zero gas emissions, offers the ability to directly convert thermal energy into electrical energy for waste heat recovery from ubiquitous temperature gradients. Historically, p-type lead chalcogenides have superior thermoelectric performance than their n-type counterpart due to the energy convergence of the valence bands. However, high-performing n-type thermoelectric materials are necessary for device application to match the p-type counterpart. PbS is an Earth-abundant and low-cost thermoelectric material, a promising alternative for PbTe and PbSe. Here, we report that the introduction of GaSb in the PbS matrix leads to conduction band convergence. This is the first example of a semiconductor dopant in the lead chalcogenides realizing the conduction band convergence rather than the more common observation of valence band convergence. GaSb can simultaneously increase the power factor and reduce the lattice thermal conductivity. As a result, a record-high average power factor PF_{avg} of ~20.4 $\mu Wcm^{-1}K^{-2}$ and figure of merit ZT_{avg} of ~0.84 from 400 K to 923 K were obtained. Our results suggest that the compound-doping strategy may be effective for all members of the lead chalcogenides, potentially leading to even higher performance in the well-studied n-type PbTe and PbSe.

GaSb Doping Facilitates Conduction Band Convergence and Improves Thermoelectric Performance in n-type PbS

Zixuan Chen,[1,2,12] Hong-Hua Cui,[3,12] Shiqiang Hao,[4] Yukun Liu,[4] Hui Liu,[5] Jing Zhou,[1] Yan Yu,[1,2,6] Qingyu Yan,[7,8] Christopher Wolverton,[4] Vinayak P. Dravid,[4] Zhong-Zhen Luo,[1,2,6,*] Zhigang Zou,[1,2,9,10] Mercouri G. Kanatzidis[11,*]

[1]Key Laboratory of Eco-materials Advanced Technology, College of Materials Science and Engineering, Fuzhou University, Fuzhou, 350108, China

[2]Fujian Science & Technology Innovation Laboratory for Optoelectronic Information of China, Fuzhou, Fujian 350108, China

[3]Mechanical and Electrical Engineering Practice Center, Fuzhou University, Fuzhou, 350108, China

[4]Department of Materials Science and Engineering, Northwestern University, Evanston, Illinois 60208, United States

[5]Beijing Advanced Innovation Center for Materials Genome Engineering, University of Science and Technology Beijing, Beijing 100083, China

[6]Key Laboratory of Advanced Materials Technologies, International (HongKong Macao and Taiwan) Joint Laboratory on Advanced Materials Technologies, College of Materials Science and Engineering, Fuzhou University, Fuzhou, Fujian, 350108, China

[7]School of Materials Science and Engineering, Nanyang Technological University, 50 Nanyang Avenue 639798, Singapore

[8]Institute of Materials Research and Engineering, A*STAR, 138634, Singapore

[9]Eco-materials and Renewable Energy Research Center, College of Engineering and Applied Sciences, Nanjing University, Nanjing, 210093, China

[10]National Laboratory of Solid State Microstructures, Nanjing University, Nanjing 210093, China.

[11]Department of Chemistry, Northwestern University, Evanston, Illinois 60208, United States

[12]These authors contributed equally: Zixuan Chen, Hong-Hua Cui

Corresponding authors: E-mail: zzluo@fzu.edu.cn (Z. Z. Luo),

E-mail: m-kanatzidis@northwestern.edu (M. G. Kanatzidis)

ABSTRACT

P-type lead chalcogenides have superior thermoelectric performance because they exhibit the energy convergence of several valence bands. However, despite the existence of two conduction bands, there has been no report about conduction band (CB) convergence for n-type counterparts because of the large energy difference between them. New strategies are required to manipulate the CBs if enhancing the electrical transport performance of n-type lead chalcogenides is to be achieved. PbS is a highly attractive member of the lead chalcogenides because of its high earth-abundance and low cost. Here, we report that the introduction of GaSb can successfully dope the PbS matrix with Ga and Sb atoms occupying the Pb site in its rock salt structure. GaSb doping leads to conduction band convergence and enlarged effective density of state mass for n-type PbS. This effect results in superior power factors and decreased lattice thermal conductivity caused by the soft phonon modes and point defect scattering of phonons. Consequently, a record-high average power factor PF_{avg} of ~20.4 $\mu Wcm^{-1}K^{-2}$ and figure of merit ZT_{avg} of ~0.84 in the temperature range of 400 K to 923 K were obtained, higher than any n- and p-type PbS-based thermoelectric materials.

Keywords: Thermoelectric, n-type PbS, GaSb, conduction band convergence, soft phonon modes

INTRODUCTION

Thermoelectric technology offers the ability to directly convert thermal energy into electrical energy holding great potential for use in waste heat recovery from ubiquitous temperature gradients. The dimensionless figure of merit evaluates the conversion efficiency of a thermoelectric material, $ZT = S^2\sigma T/\kappa_{tot}$, where S is the Seebeck coefficient, σ is the electrical conductivity, T is the absolute temperature, and κ_{tot} is the thermal conductivity consisting of electronic and lattice components, κ_{ele} and κ_{lat}.[1-8] Thus, a high ZT value will be achieved with high S, σ, and low κ_{tot}. However, improving the thermoelectric properties is a huge challenge because of the strong coupling of S, σ, and κ_{ele}. The $S^2\sigma$ is defined as the power factor (PF), which determines the electrical transport performance of thermoelectric materials and is a significant indicator for the output power (ω), as[9, 10] $\omega = \frac{1(T_H - T_C)^2}{4 \quad L} PF_{avg}$, where T_H, and T_C are the hot and cold side temperature, and L is thermoelectric leg length, respectively. Moreover, for the efficiency (η) of a practical thermoelectric device, η is defined as $\eta = [(T_H - T_C)/T_H]\,[(1 + ZT_{avg})^{1/2} - 1]/[(1 + ZT_{avg})^{1/2} + T_C/T_H]$, where ZT_{avg} is the average ZT value over the temperature range from T_C to T_H. Achieving a high ZT_{avg} is more important than ZT_{max} for efficient device operation.[11, 12]

Lead chalcogenides (PbQ, Q = Te, Se, S) are state-of-art thermoelectric materials in the intermediate temperature range (500−900 K). With the unique two valence bands (VB) electronic structure and intrinsically low thermal conductivity caused by phonon anharmonicity,[13] p-type PbTe and PbSe are the most extensively studied and achieve excellent thermoelectric performance, such as the high ZT_{avg} of ~1.70 (400−923 K) for PbTe.[14] However, for their n-type counterparts, the power factors are more challenging to improve due to the large energy difference between the two conduction bands (CB) electronic structure.[15] As a result, the ZT_{avg} value for n-type PbTe is ~1.26 (400−873 K).[8] Moreover, because of higher costs, a preferable choice over PbTe and PbSe would be the PbS.[16, 17]

Historically, although PbS displays inferior thermoelectric performance than PbTe and PbSe, PbS is an Earth-abundant and low-cost thermoelectric material (Figure S1,

Supporting information). The abundance of the Earth's S, Se, and Te elements is 420, 0.05, and 0.001 ppm, respectively.[18] Thus, with the same crystal structure and similar electronic band structure, PbS is regarded as a promising alternative for PbTe and PbSe if sufficient breakthroughs in raising its performance are achieved. Moreover, with excellent chemical stability and the highest melting temperature, PbS has the highest potential operating temperature.[19] Recent studies display improved thermoelectric properties in n-type PbS-based thermoelectric materials with peak *ZT* values ~1.2 at a high temperature via the reduction of κ_{lat}, such as nanoscale precipitates and point defects.[19] However, the more important ZT_{avg} values are not respected, such as PbS-1%Sb_2S_3-1%$PbCl_2$ (ZT_{avg} ~0.52 from 300−923 K with ZT_{max} ~1.1 at 923 K),[20] PbS-3%SrS-1%$PbCl_2$ (ZT_{avg} ~0.65 from 300−923 K with ZT_{max} ~1.2 at 923 K),[21] and $Pb_{0.95}Sb_{0.02}Cu_{0.03}$S-0.03Cu ($ZT_{avg}$ ~0.62 from 300−923 K with ZT_{max} ~1.23 at 923 K).[22] These approaches lead to the significantly reduced κ_{lat}, which is close to the amorphous limit for PbS (κ_{lat} ~0.46 $Wm^{-1}K^{-1}$)[23] at high temperatures. However, with the limited room for further reduction in κ_{lat}, we are exploring routes that boost *ZT* via increasing the *PF*.

The multiple valence bands in the electronic structure are the key to achieving High thermoelectric performance in p-type PbQ (Q = S, Se, Te). This is done by energy-converging the valence bands of PbQ using alloying strategies. By using alloying strategies, mainly on the Pb site, such as in the $Pb_{1-x}Sr_xTe$ systems, the valence bands of PbQ can be energy-converged.[24] This is effective because the *L* and *Σ* bands are close in energy (around 0.25 eV), so a small amount of Sr^{2+} doping can lower the top of the *L* band closer to the *Σ* band, resulting in an energy difference of less than 0.15 eV. This greatly increases the density of states (DOS) effective mass for holes, which enhances the Seebeck coefficient.[14] It is very difficult, however, to achieve convergence of the two conduction bands present in the electronic structures of all PbQ. The conduction band also includes two *L* and *Σ* bands, but the energy difference between these bands is greater than 0.4 eV,[25-27] and no effective methods have been found to bring them closer in energy. Here we reveal an example of how to accomplish this in PbS with the

use of two different dopants. Historically, elemental dopants have been employed to optimize the carrier concentration, band structure, and microstructure of thermoelectric materials. The examples of compound dopants are few and they generally decompose and then distribute in the matrix, such as GaSb and InSb in the PbTe matrix.[28, 29] Here, we report the significantly enhanced PF_{avg} and ZT_{avg} value in n-type PbS via the GaSb semiconductor doping. Interestingly, one Ga and one Sb atom co-occupy the Pb site in the rock-salt PbS matrix. Our first-principles electronic structure calculations indicate a conduction band convergence and enlarged effective density of state mass. The conduction band convergence leads to enhanced Seebeck coefficients and superior *PF* of ~24 $\mu Wcm^{-1}K^{-2}$ at 423 K. Especially, the PF_{avg} ~20.4 $\mu Wcm^{-1}K^{-2}$ in the temperature range of 400−923 K was obtained, which exceeds those reported for n- and p-type PbS-based materials.[21, 22, 30, 31] Consequently, a record-high ZT_{avg} of ~0.84 in the temperature range of 400−923 K rendering PbS a viable low-cost alternative for device applications.

RESULTS AND DISCUSSION

Structural Characterization. The phase structure and purity of $Pb_{1-x}(GaSb)_xS$ (x = 0, 0.1%, 0.3%, 0.6%, and 0.9%) were verified by powder X-ray diffraction (PXRD) measurement. As displayed in Figure 1a, the PXRD patterns confirmed that all samples are pure single-phase compounds and crystalized in the rock salt structure with a space group of $Fm\bar{3}m$ (PDF#78−1055). As shown in Figure 1b, the lattice parameter of $Pb_{1-x}(GaSb)_xS$ slightly increased with the GaSb dopant. The XRD patterns indicate an absence of any detectable reflections from impurity phases. In contrast, the lattice parameters are decreased when single dopants Ga- and Sb- are used to dope PbS (used here as control samples), Figure 1c. The increased lattice parameter of GaSb-doped PbS can be attributed to the substitution of Pb by Ga and Sb, agreeing with the calculated crystal structure.

Micro- and Nano-structure analysis. Back-scattered electron (BSE) scanning

electron microscopy (SEM) characterization and energy dispersive spectroscopy (EDS) analysis of $Pb_{0.997}(GaSb)_{0.003}S$ (Figure S4, Supporting information) shows a uniform contrast which indicates a single-phase region with a homogeneous distribution of Pb, S, Ga, and Sb elements. The low-magnification high-angle annular dark field scanning transmission electron microscopy (HAADF-STEM) images are formed by incoherently scattered electrons that are collected at high angles. Therefore, the image contrast is highly sensitive to variations in the atomic number of atoms. The uniform contrast in both HAADF image and the corresponding EDS maps (Figure 2a-b) reveals a homogeneous distribution of elements without detecting clusters or second phase formation. Figure 2c is a high-resolution TEM (HRTEM) image along the [110] zone axis. It shows clear lattice fringes, and no obvious defects or second phases were observed. Figure 2d presents an atomic-resolution TEM image of the region surrounded by a yellow box in Figure 2c. The revealed lattice fringes have interplanar spacings of 3.04 Å and 2.14 Å and an intersection angle of 90°, in good agreement with the expected values of the (002) and $(2\bar{2}0)$ planes of rock-salt $Pb_{0.997}(GaSb)_{0.003}S$. In addition, high-resolution HAADF-STEM characterization (Figure S6, Supporting information) was also performed on the same sample along the [100] zone axis. The observed homogeneous crystalline phase and measured atomic plane spacings are consistent with the results in Figure 2 and the expected values of the (002) and (020) planes. The structure and composition analysis at multiple length scales confirm that only one phase exists in $Pb_{0.997}(GaSb)_{0.003}S$, and the results agree with the XRD measurement.

Charge Transport Properties.

Hall Coefficient. The temperature-dependent Hall coefficient, R_H, has been measured to understand the electronic transport of $Pb_{1-x}(GaSb)_xS$ samples, as shown in Figure 3. The n-type R_H decreased with GaSb dopant content from x = 0 to x = 0.6% samples, then slightly increased for x = 0.9% samples at room temperature. Correspondingly, the n increased from 2.88×10^{19} cm^{-3} for x = 0.1% to 6.75×10^{19} for x = 0.6% samples and then slightly decreased to 6.17×10^{19} for x = 0.9% sample (Figure S7, Supporting information). The trends agree with the electrical conductivity and Seebeck coefficient

values, as presented in the next part.

Electrical Conductivity and Seebeck Coefficients. The temperature-dependent electrical conductivity of $Pb_{1-x}(GaSb)_xS$ significantly increases with GaSb content from ~41 Scm^{-1} for pure PbS and reaches the maximum value of ~2302 Scm^{-1} for $Pb_{0.994}(GaSb)_{0.006}S$ and then decrease to ~1837 Scm^{-1} for $Pb_{0.991}(GaSb)_{0.009}S$ at 300 K, Figure 4a. The electrical conductivity decreases with increasing temperature for all samples, indicating the degenerately doped semiconductors. The increasing trend is caused by the increase of n from ~2.88 × 10^{19} cm^{-3} for $Pb_{0.999}(GaSb)_{0.001}S$ to ~6.75 × 10^{19} cm^{-3} for $Pb_{0.994}(GaSb)_{0.006}S$ (Figure S7, Supporting information). The carrier mobility (μ_H) of $Pb_{1-x}(GaSb)_xS$ (Figure 3b) decreases slightly as the GaSb dopant content increases at room temperature, and decreases continuously with increasing temperature for all samples. Compared with the previous top-performing n-type PbS-based sample, $Pb_{0.93}Sb_{0.01}Sn_{0.06}S$-x%PbTe (PbS-Sb-Sn-Te),[30] $Pb_{0.98-x}Sb_{0.02}Cu_xS$-yCu (PbS-Sb-Cu),[22] PbS-x$PbCl_2$ (PbS-Cl),[20] PbS-1%$PbCl_2$-xSb_2S_3 (PbS-Cl-Sb_2S_3),[20] PbS-1%$PbCl_2$-1%Ca/SrS (PbS-Ca/SrS),[20] $Pb_{1-x}Ge_xS$,[32] and PbS-1%$PbCl_2$-xBi_2S_3 (PbS-Bi_2S_3),[20] the GaSb-doped PbS samples exhibit superior carrier electron mobility, μ_H (186.0 – 229.2 $cm^2V^{-1}s^{-1}$ with n from ~2.88 to 6.75 × 10^{19} cm^{-3}) at room temperature (Figure S8, Supporting information).

The temperature-dependent Seebeck coefficients for $Pb_{1-x}(GaSb)_xS$ are outlined in Figure 4b. The negative values of Seebeck coefficients indicate that the samples are n-type materials, and the electron is the dominant carrier over the entire temperature range, which is consistent with the negative values of the R_H (Figure 3b). The undoped PbS displays the highest Seebeck coefficients above −300 μVK^{-1} in the measured temperature range. For GaSb doped samples, the Seebeck coefficient decreases from −123 to −95 μVK^{-1} with the GaSb content increasing from x = 0.1% to 0.9% at 300 K. The Seebeck coefficient increases with the rise in the temperature for all GaSb doped samples and reach a maximum of −310 μVK^{-1} at 863 K for x = 0.1% sample.

Based on the Seebeck coefficient being a function of the carrier concentration n, we constructed the Pisarenko relation for $Pb_{1-x}(GaSb)_xS$ at 300 K, shown in Figure 4c. The

purple curve calculated for n-type PbS based on the single parabolic band (SPB) model with a density of state (DOS) effective mass for electrons of 0.45 m_e, where m_e is the free electron mass. Compared with the Ga-doped PbS,[31] Sb-doped PbS[33] and Ga-In co-doped PbS,[31] the GaSb semiconductor-doped PbS samples have significantly enhanced density of states (DOS) effective mass for electrons (m_0) of approximately 0.7 m_e, resulting in noticeable increases in the absolute Seebeck coefficient values. Moreover, compared with other n-type dopants, such as Ga,[31] Sb, Ga-In,[31] and In,[34] the temperature-dependent Seebeck coefficient of GaSb-doped PbS has the highest value with the closed carrier concentration (~3.0×10^{19} cm^{-3}) over the entire temperature range (Figure 5). For example, for a given carrier concentration of ~3.0×10^{19} cm^{-3} the Seebeck coefficient is enhanced from −101 μVK^{-1} (~2.7×10^{19} cm^{-3}) or −83 μVK^{-1} (~3.3×10^{19} cm^{-3}) to −123 μVK^{-1} (~2.9×10^{19} cm^{-3}) at room temperature, marking the ~22% to 48% increase. The results indicate that GaSb doping can improve the multi-band character of the conduction band structure of PbS. Details on the possible origins are discussed in the DFT calculations given later.

Power Factor. Based on the measured electrical conductivity and Seebeck coefficients, the temperature-dependent *PF* of $Pb_{1-x}(GaSb)_xS$ samples is calculated and shown in Figure 4d. Because of enhanced electrical conductivities and the high Seebeck coefficient for GaSb doped samples, the *PF* exhibits an ultrahigh value of above 10 $\mu Wcm^{-1}K^{-2}$ across the whole temperature range. Remarkably, the $Pb_{0.997}(GaSb)_{0.003}S$ has the highest power factor of ~24 $\mu Wcm^{-1}K^{-2}$ at 423 K. Moreover, according to the formula, $PF_{avg} = \frac{1}{T_H - T_C}\int_{T_C}^{T_H} PF \mathrm{d}T$, the record high PF_{avg} of ~20.4 $\mu Wcm^{-1}K^{-2}$ in the temperature range of 400−923 K was obtained compared with the top-performing n-type PbS-based thermoelectric materials (Figure 6).[21, 22, 30, 31]

Thermal Conductivity. As shown in Figure 7A, the temperature-dependent total thermal conductivity κ_{tot} values for the $Pb_{1-x}(GaSb)_xS$ are decreased with temperatures. With the increase of GaSb dopant, the κ_{tot} increases with GaSb content from ~2.58 $Wm^{-1}K^{-1}$ for x = 0 and reaches the highest value of ~3.35 $Wm^{-1}K^{-1}$ for x = 0.6 samples, and then decrease to ~3.23 $Wm^{-1}K^{-1}$ for x = 0.9 sample at 300 K. These trends are

agreed with the n with GaSb dopant content. Also, the n results in a significant rise in electronic part κ_{ele} according to the Wiedemann-Franz relation,[35] $\kappa_{ele} = L\sigma T = Lne\mu_H T$ (where L is the Lorenz number, obtained by $L = 1.5 + \exp[-|S|/116] \times 10^{-8}$ V^2K^{-2}) as shown in Figure S9 (Supporting information).

The lattice thermal conductivity (κ_{lat}) is obtained by subtracting the κ_{ele} from the κ_{tot}. As shown in Figure 7b, GaSb doping will decrease the κ_{lat} and further reduce with temperatures, which is the most common for semiconductors due to typical Umklapp phonon-phonon scattering above the Debye temperature. In detail, $Pb_{0.994}(GaSb)_{0.006}S$ has the lowest ~1.96 $Wm^{-1}K^{-1}$ at 300 K, a reduction of 23% than undoped PbS (κ_{lat} ~2.56 $Wm^{-1}K^{-1}$). Moreover, this composition reaches ~0.88 $Wm^{-1}K^{-1}$ at 923 K. As shown in Figure S10 (Supporting information), the κ_{lat} of $Pb_{0.994}(GaSb)_{0.006}S$ sample has relatively low values compared to Cu-doped,[36] Cl-doped,[37] Sb-Cl co-doped[38], Sb-Cu co-doped,[22] Ga-doped,[31] and Sb-doped[39] n-type PbS-based thermoelectric materials. Obviously, GaSb doping has a strong impact on reducing the κ_{lat} of PbS. To understand the significant reduction of κ_{lat} caused by GaSb alloying, the crystal structure from the calculation was investigated and discussed below.

Electronic Structure DFT Calculations. We investigated the electronic band structure of GaSb-doped PbS. As displayed in Figure 8, the conduction band of GaSb-doped PbS is significantly different from pure PbS, Ga-doped PbS, and Sb-doped PbS. The density of states of the first conduction band minimum is contributed from Ga 4s, Sb 5p, and Pb 6p states, Figures 8g and 8h. The second conduction minimum, around 0.15 eV above the Fermi level, is mainly contributed from Sb 5p stats. As shown in Figure 9, the GaSb-doping can significantly reduce the conduction band energy difference (ΔE_c) between the L and Σ bands of PbS. Compared to the ΔE_c values of ~0.34 eV for pure PbS, ~0.32 eV for Ga-doped PbS, and ~0.25 eV for Sb-doped PbS, the GaSb-doped PbS has the lowest ΔE_c ~0.15 eV, which is equal to the value of valence band energy difference (ΔE_v) between the L and Σ bands for PbTe.[14] It is well known that the low ΔE_v ~0.15 eV results in excellent electrical transport properties for p-type PbTe because the Σ band can also contribute to hole transport.[24] Compared to 0.52 m_e for Ga and 0.54

m_e for Sb -doped PbS, another important effect of the GaSb-doping is the enhanced density of state effective mass to ~0.64 m_e, which is very close to the experimental value of 0.7 m_e, see Table S1 (Supporting information). The enhanced effective mass accounts for the experimental observation of the enhanced Seebeck coefficient.

To understand the significantly reduced κ_{lat} of GaSb-doped PbS, we evaluated phonon vibrations of GaSb-doped PbS. By comparing the phonon dispersions with our previous pure PbS dispersions, we find that the calculated phonon velocity and longitudinal Debye temperature of the GaSb-doped case are lower than those in PbS itself. Specifically, the average phonon velocity of pure PbS is 2743 ms^{-1}, while the GaSb-doped PbS is decreased to 2322 ms^{-1}. The average longitudinal Debye temperature of pure PbS is ~69 K, while the GaSb-doped PbS is ~37 K. Clearly, the decrease of all these parameters originates in the low-frequency vibrations of the next nearest (NN) neighbor Pb, as shown in the projected phonon density of states (PDOS).

Similar to our previous work PbSe-GeSe,[40] the GaSb-doped sample exhibited very low-frequency vibrations around Gamma (Γ) point (Figure 10), which are expressed as softened optical modes in phonon dispersions. Furthermore, the strong attraction of GaSb to the nearest S atoms induces longer bonds between these S atoms and the next nearest neighbor Pb atoms. The enlarged Pb coordination environment of these next nearest neighbors results in some even lower frequency vibrations. This is reflected in the PDOS shift to low frequencies relative to those of Pb atoms that are residing farther away from GaSb (not nearest neighbors). Therefore, the GaSb-doped PbS not only exhibits softened optical vibrations but also creates a defect-induced local strain field that strongly influences the next nearest neighbor Pb atoms causing them to engage in lower frequency vibrations. All these effects contribute to the remarkably lower κ_{lat} observed (Figure S12, Supporting information).

Figure of Merit. The temperature-dependent figures of merit, *ZT*, for $Pb_{1-x}(GaSb)_xS$ are displayed in Figure 11a. Combined with the significantly improved power factor and reduced κ_{lat}, $Pb_{0.997}(GaSb)_{0.003}S$ shows a high room-temperature *ZT* of ~0.21 and a maximum *ZT* of ~1.12 at 923 K, nearly 4 and 7 times that of pristine PbS, respectively.

The ZT_{avg} was calculated as follows: $ZT_{avg} = \frac{1}{T_H - T_C}\int_{T_C}^{T_H} ZT \mathrm{d}T$ to evaluate the potential performance of this material in a thermoelectric module. The GaSb-doped $Pb_{0.997}(GaSb)_{0.003}S$ has an excellent ZT_{avg} ~0.84 in the temperature range of 400 K to 923 K. Combined with the p-type PbS composition with the highest ZT_{avg} ~0.65,[19] an ideal efficiency of ~9.4% in PbS-based materials is estimated with T_H = 923 K and T_C = 400 K. The ZT_{avg} values for $Pb_{0.997}(GaSb)_{0.003}S$ outperform those of any reported both n- and p-type PbS-based materials (Figure 11b). ZT_{avg} has a decisive role in a thermoelectric device.[19, 20, 31, 41] The engineering ZT (ZT_{eng}) and engineering PF (PF_{eng}) were also calculated since they can predict the conversion efficiency of the device.[52] The GaSb-doped $Pb_{0.997}(GaSb)_{0.003}S$ has a PF_{eng} ~0.93 $Wm^{-1}K^{-1}$ and ZT_{eng} ~0.57 in the temperature range of 400 K to 923 K. The comparison of PF_{eng} and ZT_{eng} values with previous PbS compounds is illustrated in Figure 12. The results indicate that $Pb_{0.997}(GaSb)_{0.003}S$ compound is a competitive PbS-based material for assembling the device.

CONCLUSIONS

Doping PbS with GaSb can simultaneously increase the power factor and reduce the lattice thermal conductivity (κ_{lat}) of n-type samples by bringing the conduction band closer together and softening the phonon modes. The GaSb dopant optimizes carrier concentration by occupying the Pb site along with GaSb, improves the effective density of states and Seebeck coefficient through convergence of the conduction band, and reduces κ_{lat} through enhanced phonon scattering due to soft phonon modes and point defects, resulting in significantly improved electrical transport properties. As a result, a record high PF_{avg} of ~20.4 $\mu Wcm^{-1}K^{-2}$ in the temperature range of 400−923 K and a record high ZT_{avg} of ~0.84 can be achieved in $Pb_{0.997}(GaSb)_{0.003}S$. For device application, high efficiency of ~9.4% in PbS-based materials is estimated with T_H = 923 K and T_C = 400 K. Therefore, the abundant PbS could be a competitive choice for use in intermediate-temperature thermoelectric power conversion applications. Doping thermoelectric materials with additional compounds has the potential to improve their

performance by optimizing the electronic band structure and simultaneously enhancing phonon scattering. Achieving conduction band convergence in lead chalcogenides has proven to be challenging. To our knowledge, this is the first instance of effective convergence, suggesting that the compound-doping strategy may be effective for all members of the family, potentially leading to even higher performance in the well-studied n-type PbTe and PbSe.

Author contribution

Z. L., Z. Z., and M. G. K. conceived and planned the experiments. Z. C. and H. C. prepared the samples and carried out thermoelectric experiments. Y. L. and V. P. D. conducted TEM measurements of the samples. S. H. and C. W. carried out the DFT calculations. Z. L., Z. Z., and M. G. K. interpreted all results and wrote and edited the manuscript. All authors have reviewed, discussed, and approved the results and conclusions of this article.

Conflicts of interest

The authors declare no conflict of interest.

ACKNOWLEDGMENTS

This work was supported in part by the National Key Research and Development Program of China (2020YFA0710303). At Northwestern work was supported in part by the Department of Energy, Office of Science, Basic Energy Sciences under grant DE-SC0014520 (sample synthesis, TEM measurements, and DFT calculations). This study was supported in part by the National Natural Science Foundation of China (52102218, U1905215, and 52072076), the Fujian Science & Technology Innovation Laboratory for Optoelectronic Information of China (2021ZZ127), and the Natural Science Foundation of Fujian Province of China (2021J01594). The authors acknowledge the Minjiang Scholar Professorship (GXRC-21004), the access to facilities for high-performance computational resources at Northwestern University and

Singapore MOE AcRF Tier 1 RG128/21, Singapore A*STAR project A19D9a0096.

References

1. L.-D. Zhao, S. H. Lo, Y. Zhang, H. Sun, G. Tan, C. Uher, C. Wolverton, V. P. Dravid and M. G. Kanatzidis, *Nature*, 2014, **508**, 373-377.
2. G. Tan, L.-D. Zhao and M. G. Kanatzidis, *Chem. Rev.*, 2016, **116**, 12123-12149.
3. B. Jiang, W. Wang, S. Liu, Y. Wang, C. Wang, Y. Chen, L. Xie, M. Huang and J. He, *Science*, 2022, **377**, 208-213.
4. T. Zhu, Y. Liu, C. Fu, J. P. Heremans, J. G. Snyder and X. Zhao, *Adv. Mater.*, 2017, **29**, 1605884.
5. A. J. Minnich, M. S. Dresselhaus, Z. F. Ren and G. Chen, *Energy Environ. Sci.*, 2009, **2**, 466-479.
6. G. J. Snyder and E. S. Toberer, *Nat. Mater.*, 2008, **7**, 105-114.
7. L.-D. Zhao, G. Tan, S. Hao, J. He, Y. Pei, H. Chi, H. Wang, S. Gong, H. Xu, V. P. Dravid, C. Uher, G. J. Snyder, C. Wolverton and M. G. Kanatzidis, *Science*, 2016, **351**, 141-144.
8. Z.-Z. Luo, S. Cai, S. Hao, T. Bailey, Y. Luo, W. Luo, Y. Yu, C. Uher, C. M. Wolverton, V. Dravid, Z. Zou, Q. Yan and M. G. Kanatzidis, *Energy Environ. Sci.*, 2022, **15**, 368-375.
9. S. El Oualid, F. Kosior, A. Dauscher, C. Candolfi, G. Span, E. Mehmedovic, J. Paris and B. Lenoir, *Energy Environ. Sci.*, 2020, **13**, 3579-3591.
10. T. Xu, A.-Y. Haruna, Z. Ma, W. Li, J. Li, Y. Luo, D. Zhang and J. Yang, *Chem. Mater.*, 2021, **33**, 8097-8105.
11. Q. Yan and M. G. Kanatzidis, *Nat. Mater.*, 2022, **21**, 503-513.
12. M. Wu, H. H. Cui, S. Cai, S. Hao, Y. Liu, T. P. Bailey, Y. Zhang, Z. Chen, Y. Luo, C. Uher, C. Wolverton, V. P. Dravid, Y. Yu, Z. Z. Luo, Z. Zou, Q. Yan and M. G. Kanatzidis, *Adv. Energy Mater.*, 2023, **13**, 2203325.
13. Z.-Z. Luo, X. Zhang, X. Hua, G. Tan, T. P. Bailey, J. Xu, U. Uher, C. Wolcerton, V. P. Dravid, Q. Yan and M. G. Kanatzidis, *Adv. Funct. Mater.*, 2018, **28**, 1801617.
14. G. Tan, F. Shi, S. Hao, L.-D. Zhao, H. Chi, X. Zhang, C. Uher, C. Wolverton, V. P. Dravid and M. G. Kanatzidis, *Nat. Commun.*, 2016, **7**, 12167.
15. A. Bali, H. Wang, G. J. Snyder and R. C. Mallik, *J. Appl. Phys.*, 2014, **116**, 033707.
16. Z. Hu and S. Gao, *Chem. Geol.*, 2008, **253**, 205-221.
17. Y. You, X. Su, S. Hao, W. Liu, Y. Yan, T. Zhang, M. Zhang, C. M. Wolverton, M. Kanatzidis and X. Tang, *J. Mater. Chem. A*, 2018, **6**, 15123-15131.
18. Z.-Z. Luo, S. Cai, S. Hao, T. P. Bailey, H. Xie, T. J. Slade, Y. Liu, Y. Luo, Z. Chen, J. Xu, W. Luo, Y. Yu, C. Uher, C. Wolverton, V. P. Dravid, Z. Zou, Q. Yan and M. G. Kanatzidis, *J. Am. Chem. Soc.*, 2022, **144**, 7402-7413.
19. L.-D. Zhao, J. He, C.-I. Wu, T. P. Hogan, X. Zhou, C. Uher, V. P. Dravid and

M. G. Kanatzidis, *J. Am. Chem. Soc.*, 2012, **134**, 7902-7912.
20. L. D. Zhao, S. H. Lo, J. He, H. Li, K. Biswas, J. Androulakis, C. I. Wu, T. P. Hogan, D. Y. Chung, V. P. Dravid and M. G. Kanatzidis, *J. Am. Chem. Soc.*, 2011, **133**, 20476-20487.
21. Z. Hou, Y. Qiu, D. Ren, Z. Huang and L.-D. Zhao, *J. Solid State Chem.*, 2019, **280**, 120995.
22. M. Zhao, C. Chang, Y. Xiao, R. Gu, J. He and L.-D. Zhao, *J. Alloys Compd.*, 2018, **781**, 820-830
23. R. Cheng, D. Wang, H. Bai, J. Wu, W. Liu, L.-D. Zhao, X. Tang and G. Tan, *Acta. Mater.*, 2021, **220**, 117337.
24. K. Biswas, J. He, Q. Zhang, G. Wang, C. Uher, V. P. Dravid and M. G. Kanatzidis, *Nat. Chem.*, 2011, **3**, 160-166.
25. J. Sun, Y. Zhang, Y. Fan, X. Tang and G. Tan, *Chem. Eng. J.* 2022, **431**, 133699.
26. D. Wang, Y. Qin, S. Wang, Y. Qiu, D. Ren, Y. Xiao and L.-D. Zhao, *Ann. Phys.*, 2020, **532**, 1900421.
27. D. Parker and D. J. Singh, *Phys. Rev. B*, 2010, **82**, 035204.
28. S. Sarkar, X. Hua, S. Hao, X. Zhang, T. P. Bailey, T. J. Slade, P. Yasaei, R. J. Korkosz, G. Tan, C. Uher, V. P. Dravid, C. Wolverton and M. G. Kanatzidis, *Chem. Mater.*, 2021, **33**, 1842-1851.
29. J. Zhang, D. Wu, D. He, D. Feng, M. Yin, X. Qin and J. He, *Adv. Mater.*, 2017, **29**, 1703148.
30. Y. Xiao, D. Wang, Y. Zhang, C. Chen, S. Zhang, K. Wang, G. Wang, S. J. Pennycook, G. J. Snyder, H. Wu and L.-D. Zhao, *J. Am. Chem. Soc.*, 2020, **142**, 4051-4060.
31. Z.-Z. Luo, S. Hao, S. Cai, T. P. Bailey, G. Tan, Y. Luo, I. Spanopoulos, C. Uher, C. Wolverton, V. P. Dravid, Q. Yan and M. G. Kanatzidis, *J. Am. Chem. Soc.*, 2019, **141**, 6403-6412.
32. E. Rathore, R. Juneja, D. Sarkar, S. Roychowdhury, M. Kofu, K. Nakajima, A. K. Singh and K. Biswas, *Mater. Today Energy*, 2022, **24**, 100953.
33. B. Jiang, X. Liu, Q. Wang, J. Cui, B. Jia, Y. Zhu, J. Feng, Y. Qiu, M. Gu, Z. Ge and J. He, *Energy Environ. Sci.*, 2020, **13**, 579-591.
34. R. Cheng, S. Hao, J. Li, H. Bai, S. Xie, Y. Gong, W. Liu, J. Wu, G. Tan and X. Tang, *ACS Appl. Mater. Interfaces*, 2020, **12**, 14203-14212.
35. H.-S. Kim, Z. M. Gibbs, Y. Tang, H. Wang and G. J. Snyder, *APL Mater.*, 2015, **3**, 041506.
36. Y. Qin, T. Hong, B. Qin, D. Wang, W. He, X. Gao, Y. Xiao and L.-D. Zhao, *Adv. Funct. Mater.*, 2021, **31**, 2102185.
37. H. Wang, E. Schechtel, Y. Pei and G. J. Snyder, *Adv. Energy Mater.*, 2013, **3**, 488-495.
38. J. Yang, X. Zhang, G. Liu, L. Zhao, J. Liu, Z. Shi, J. Ding and G. Qiao, *Nano Energy*, 2020, **74**, 104826.
39. M. Zhao, C. Chang, Y. Xiao and L.-D. Zhao, *J. Alloys Compd.*, 2018, **744**, 769-777.
40. Z.-Z. Luo, S. Hao, X. Zhang, X. Hua, S. Cai, G. Tan, T. P. Bailey, R. Ma, C.

Uher, C. Wolverton, V. P. Dravid, Q. Yan and M. G. Kanatzidis, *Energy Environ. Sci.*, 2018, **11**, 3220-3230.
41. L.-D. Zhao, J. He, S. Hao, C.-I. Wu, T. P. Hogan, C. Wolverton, V. P. Dravid and M. G. Kanatzidis, *J. Am. Chem. Soc.*, 2012, **134**, 16327-16336.
42. Z.-Y. Wang, J. Guo, J. Feng and Z.-H. Ge, *J. Solid State Chem.*, 2021, **297**.
43. X. G. Hu, W. K. He, D. Y. Wang, B. F. Yuan, Z. W. Huang and L.-D. Zhao, *Scr. Mater.*, 2019, **170**, 99-105.
44. L. Peng, S. Yang, T.-R. Wei, P. Qiu, J. Yang, Z. Zhang, X. Shi and L. Chen, *J. Materiomics*, 2021, **8**, 656-661.
45. B. Ge, H. Lee, C. Zhou, W. Lu, J. Hu, J. Yang, S.-P. Cho, G. Qiao, Z. Shi and I. Chung, *Nano Energy*, 2022, **94**, 106941.
46. Y. X. Chen, A. Yamamoto and T. Takeuchi, *J. Alloys Compd.*, 2017, **695**, 1631-1636.
47. G. J. Tan, S. G. Hao, J. Zhao, C. Wolverton and M. G. Kanatzidis, *J. Am. Chem. Soc.*, 2017, **139**, 6467-6473.
48. B. Jiang, Y. Yu, J. Cui, X. Liu, L. Xie, J. Liao, Q. Zhang, Y. Huang, S. Ning, B. Jia, B. Zhu, S. Bai, L. Chen, S. J. Pennycook and J. He, *Science*, 2021, **371**, 830-834.
49. H. Wang, S. Zheng, H. Wu, X. Xiong, Q. Xiong, H. Wang, Y. Wang, B. Zhang, X. Lu, G. Han, G. Wang and X. Zhou, *Small*, 2021, **18**, 2104592.
50. G. Guélou, V. Pavan Kumar, V. Carnevali, O. I. Lebedev, B. Raveau, C. Couder, C. Prestipino, P. Lemoine, B. Malaman, J. Juraszek, C. Candolfi, B. Lenoir, R. Al Rahal Al Orabi, M. Fornari and E. Guilmeau, *Chem. Mater.*, 2021, **33**, 9425-9438.
51. K. Lohani, H. Nautiyal, N. Ataollahi, K. Maji, E. Guilmeau and P. Scardi, *ACS Appl. Energy Mater.*, 2021, **4**, 12604-12612.
52. H.-S. Kim, W. Liu, G. Chen, C.-W. Chu and Z. Ren, *Proc. Natl. Acad. Sci. U. S. A.*, 2015, **112**, 8205-8210.

Figures

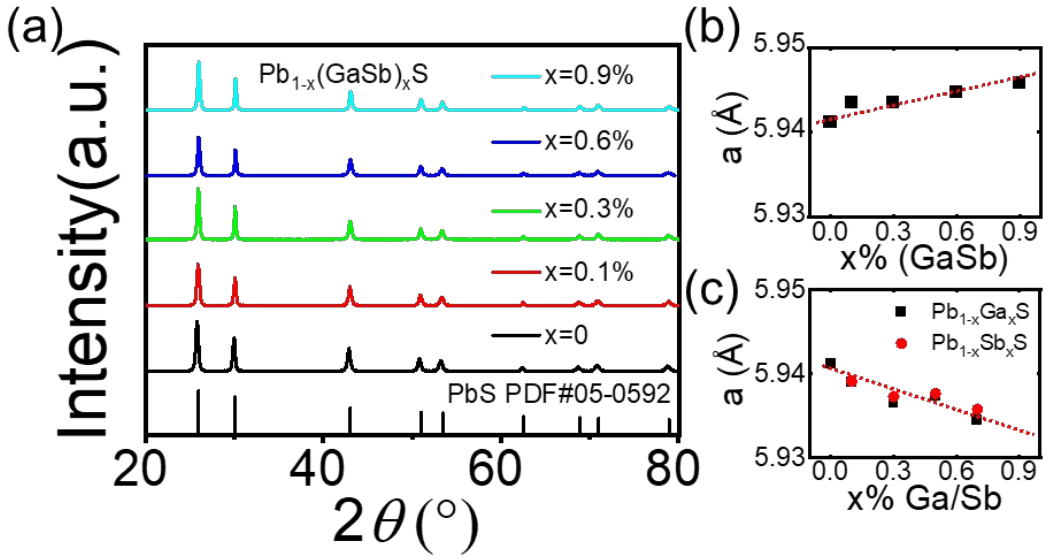

Figure 1. (a) PXRD patterns of $Pb_{1-x}(GaSb)_xS$ (x = 0, 0.1%, 0.3%, 0.6%, and 0.9%), with all peaks indexed by the PbS cubic phase (JCPDS 78−1055); (b) Refined lattice parameters of $Pb_{1-x}(GaSb)_xS$ (x = 0, 0.1%, 0.3%, 0.6%, and 0.9%) as a function of GaSb semiconductor content, indicating an expansion of the lattice and (c) Refined lattice parameters of $Pb_{1-x}Ga_xS$ and $Pb_{1-x}Sb_xS$ (x = 0, 0.1%, 0.3%, 0.5%, and 0.7%) as a function of Ga or Sb dopants, indicating a contraction of the lattice. The short dotted line is a guide to the eye.

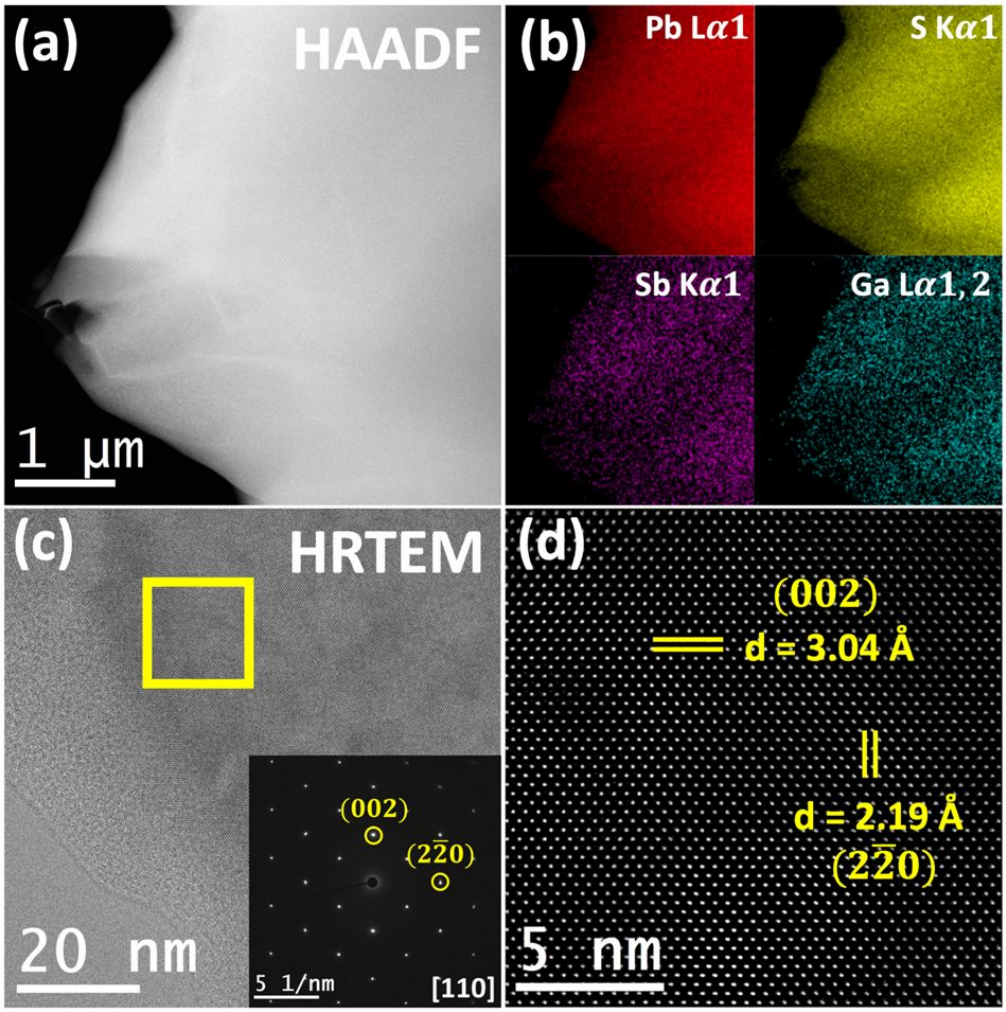

Figure 2. S/TEM analysis of the $Pb_{0.997}(GaSb)_{0.003}S$ sample. (a) High-angle annular dark field (HAADF) image of the specimen; (b) Energy dispersive spectroscopy (EDS) mapping of the region shown in (a); (c) High-resolution transmission electron microscopy (HRTEM) image along the [110] zone axis, with inset as the corresponding selected area electron diffraction (SAED) pattern; (d) Atomic-resolution TEM image of the region surrounded by the yellow box in (c) with atomic plane spacings labeled.

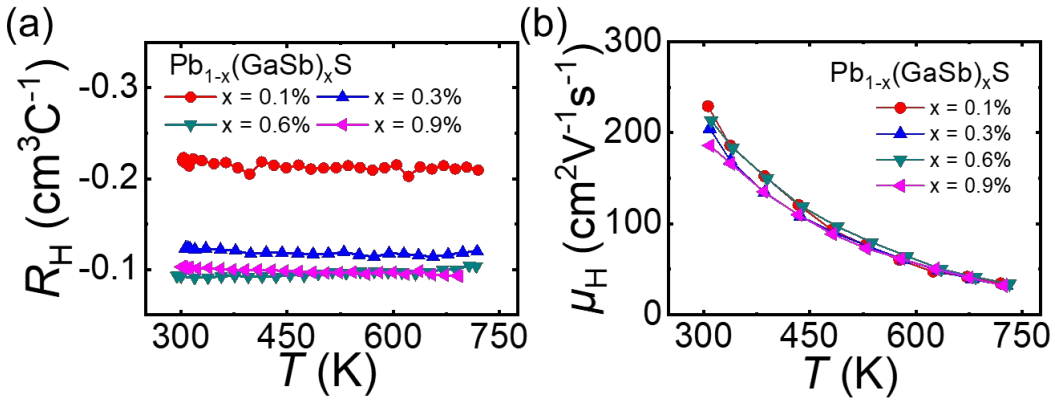

Figure 3. Temperature-dependent Hall coefficients, R_H and carrier mobility, μ_H for $Pb_{1-x}(GaSb)_xS$ (x = 0.1%, 0.3%, 0.6%, and 0.9%) samples.

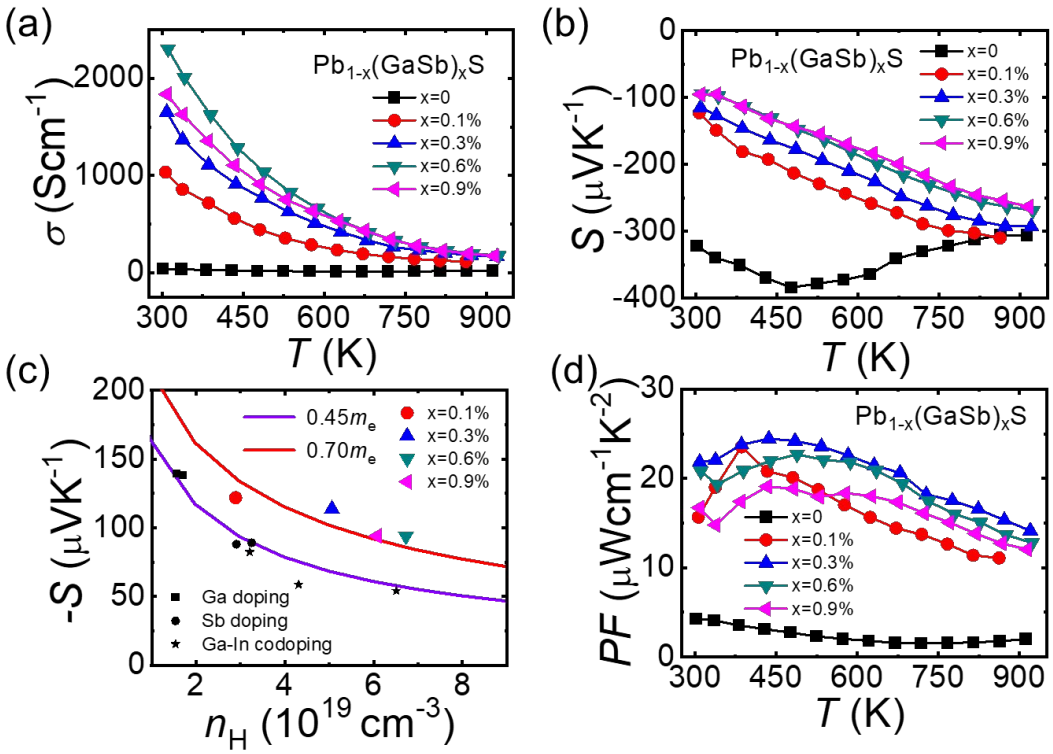

Figure 4. Thermoelectric properties as a function of temperature for $Pb_{1-x}(GaSb)_xS$ (x = 0, 0.1%, 0.3%, 0.6%, and 0.9%): (a) Electrical conductivity, σ; (b) Seebeck coefficient, S; (c) Seebeck coefficient as a function of n at room temperature. The solid purple and red curves are the theoretical Pisarenko curves for n-type PbS with the effective mass of electrons of 0.45 m_e and 0.6 m_e, respectively; and (d) Power Factor, PF.

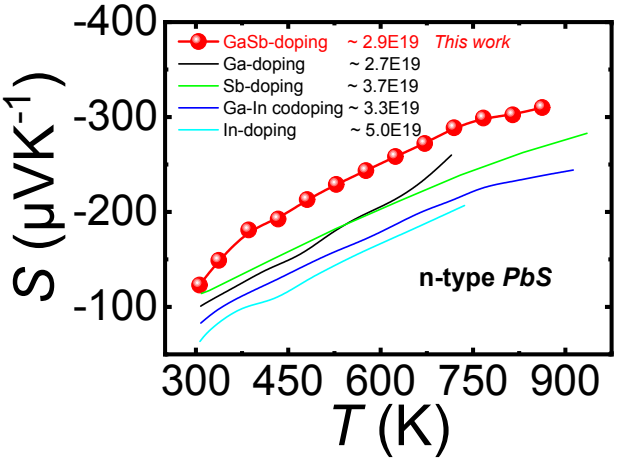

Figure 5. Comparison of temperature-dependent Seebeck coefficient of GaSb-doped PbS with other n-type PbS dopants, such as Ga,[31] Sb, Ga-In,[31] and In.[34]

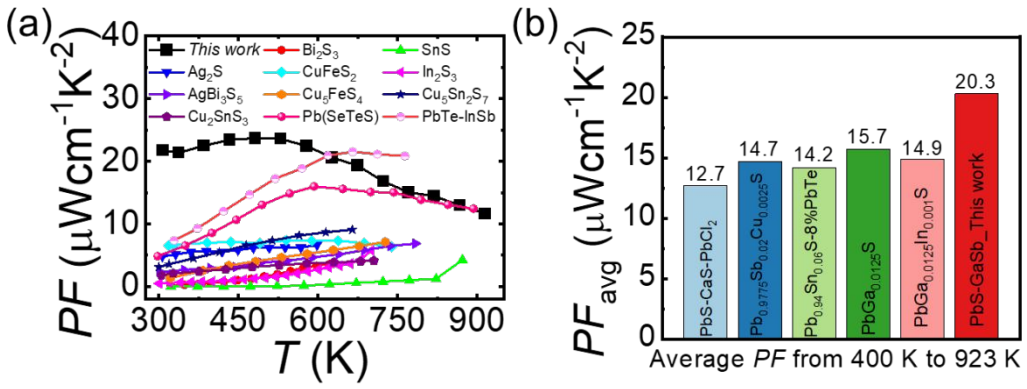

Figure 6. Comparison of power factor, *PF* in this work ($Pb_{0.997}(GaSb)_{0.003}S$) with the state-of-the-art previous n-type (Bi_2S_3-1%$NbCl_5$ (Bi_2S_3),[42] $SnS_{0.98}Br_{0.02}$ (SnS),[43] $Ag_2S_{0.7}Te_{0.3}$ (Ag_2S),[44] $Cu_{0.96}In_{0.04}FeS_2$ ($CuFeS_2$),[45] $In_{1.95}Mg_{0.05}S_3$ (In_2S_3),[46] $AgBi_3(S_{0.9967}Cl_{0.0033})_5$ ($AgBi_3S_5$),[47] $Pb_{0.89}Sb_{0.012}Sn_{0.1}Se_{0.5}Te_{0.25}S_{0.25}$ (Pb(SeTeS), the ZT_{max} ~1.8@900 K),[48] and PbTe-4%InSb (PbTe-InSb, the ZT_{max} ~1.83@773 K)[29]), and p-type ($Cu_5FeS_{3.8}Se_{0.2}$ (Cu_5FeS_4),[49] $Cu_{5.133}Sn_{1.866}S_{6.65}Cl_{0.35}$ ($Cu_5Sn_2S_7$),[50] and Cu_2SnS_3[51]) chalcogenide thermoelectric materials and (b) The comparison of PF_{avg} values at 400–923 K for top-performing n-type PbS-based thermoelectric materials.[21, 22, 30, 31]

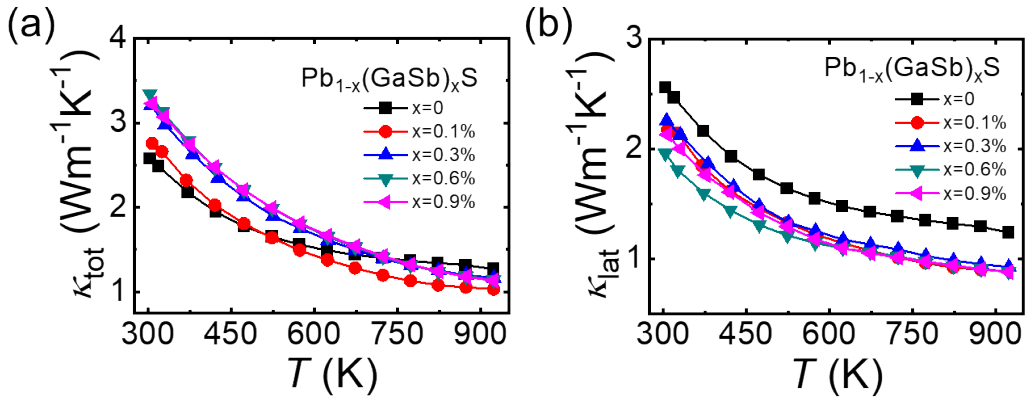

Figure 7. Thermal properties as a function of temperature for $Pb_{1-x}(GaSb)_xS$ (x = 0, 0.1%, 0.3%, 0.6%, and 0.9%) total thermal conductivity, κ_{tot} (a) and lattice thermal conductivity, κ_{lat} (b).

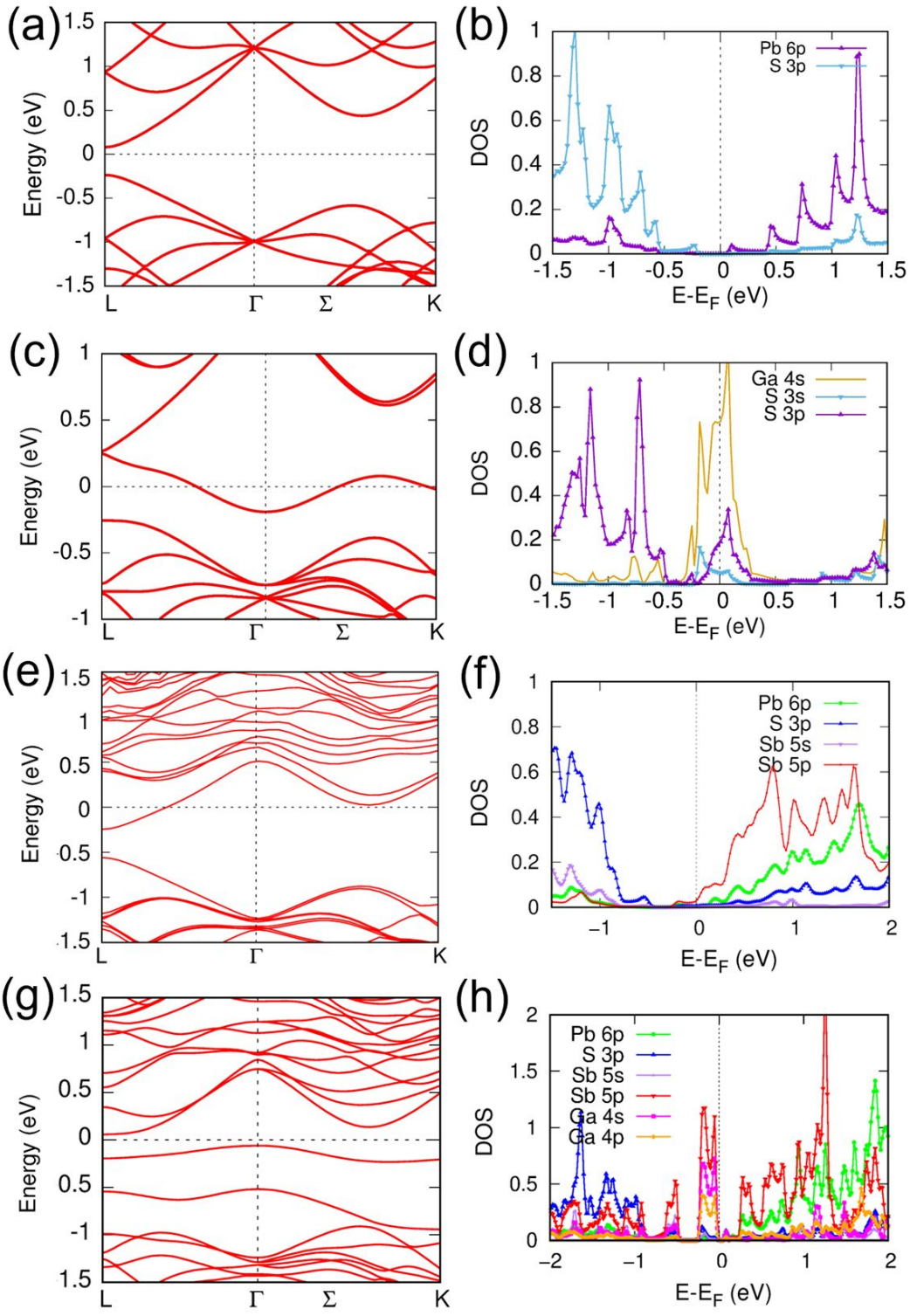

Figure 8. Electronic band structures and corresponding density of states (DOS) for pure PbS (a and b), Ga-doped PbS (c and d), Sb-doped PbS (e and f), and GaSb-doped PbS (g and h).

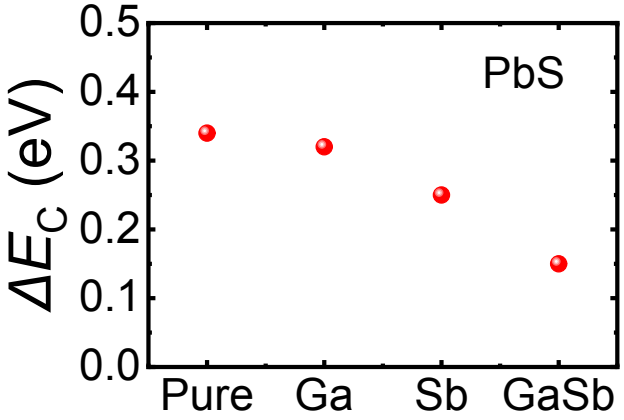

Figure 9. The calculated conduction band energy difference (ΔE_c) between the L and Σ bands of pure PbS (pure), Ga-doped PbS (Ga), Sb-doped PbS (Sb), and GaSb-doped PbS (GaSb).

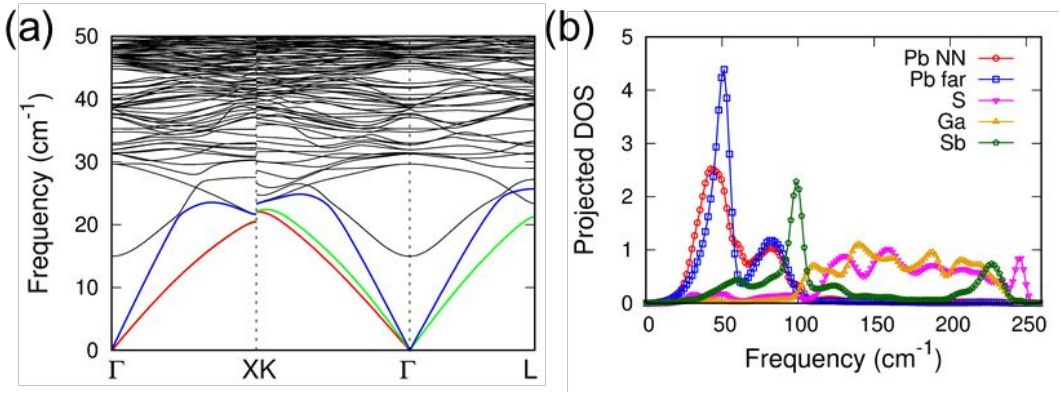

Figure 10. Phonon dispersion curves (acoustic branches: red and green curves for the transverse and blue curves for the longitudinal) (a) and corresponding the projected phonon density of states (DOS) (b) for GaSb-doped PbS. There have low-frequency optical vibration modes with a frequency of ~15 cm^{-1} at the Γ point in a, which is beneficial for reducing the κ_{lat}. According to the projected DOS in b, this low-frequency optical model is caused by the next nearest neighbor Pb.

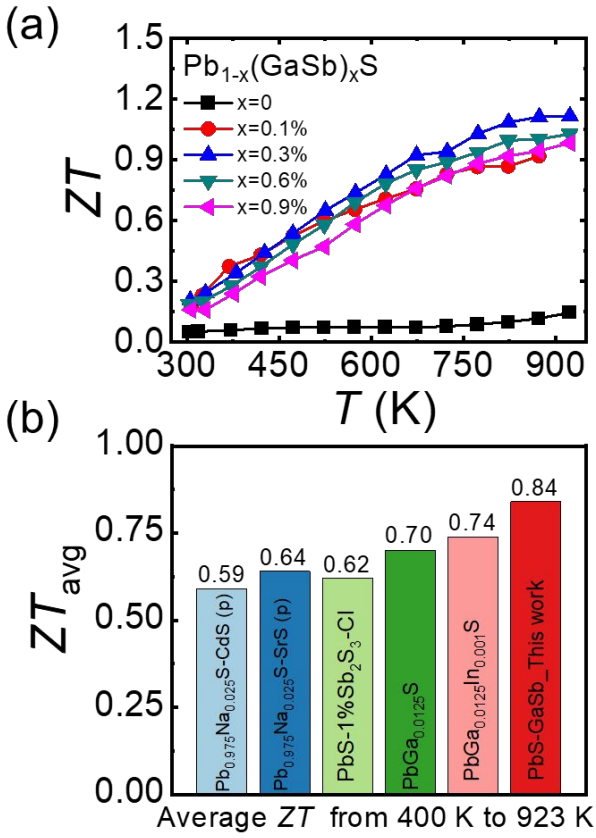

Figure 11. (a) Figure of merit, *ZT*, as a function of temperature for $Pb_{1-x}(GaSb)_xS$ (x = 0, 0.1%, 0.3%, 0.6%, and 0.9%), and (b) comparison of ZT_{avg} values at 400–923 K the state-of-the-art n-type PbS-based thermoelectric materials.[19, 20, 31, 41]

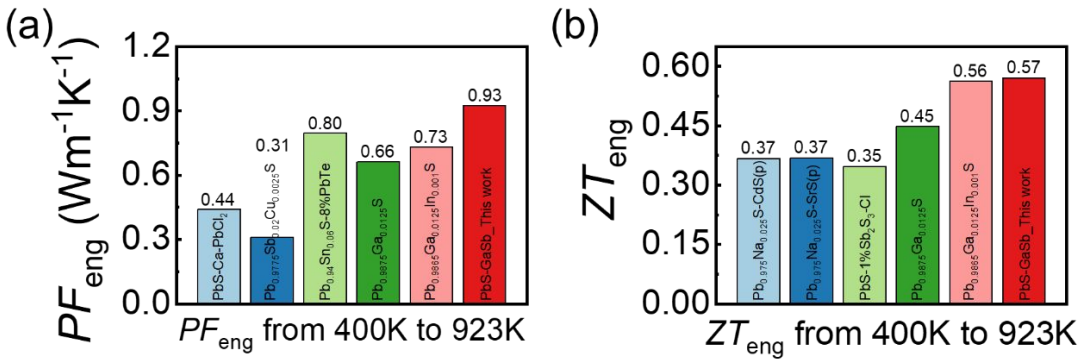

Figure 12. The comparison of PF_{eng} (a) and ZT_{eng} (b) values at 400–923 K for top-performing n-type PbS-based thermoelectric materials.

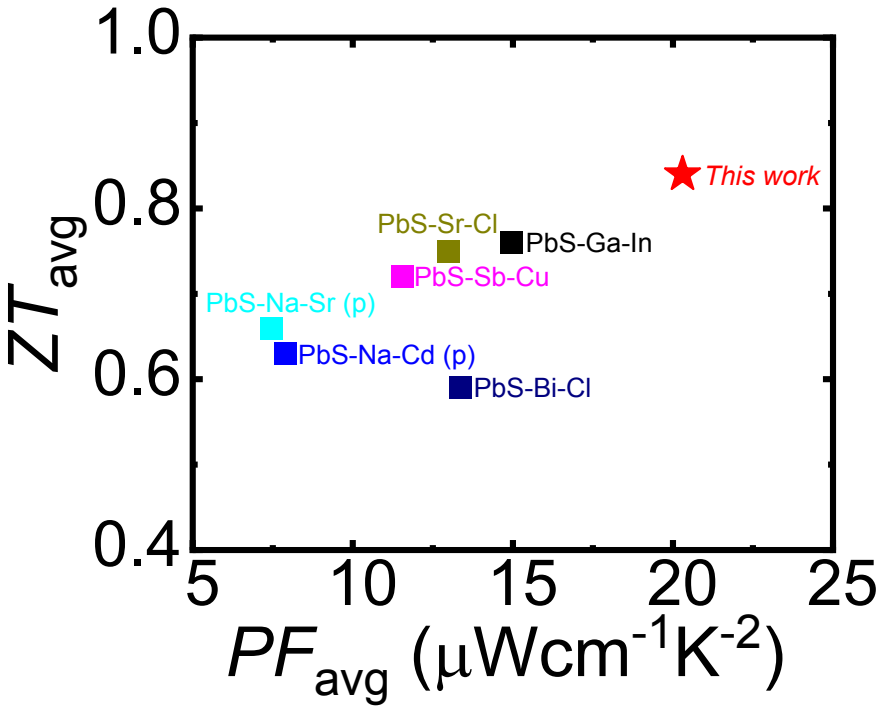

Figure 13. Comparison of the PF_{avg} and ZT_{avg} values for $Pb_{0.95}Sb_{0.02}Cu_{0.03}S$-0.03Cu (PbS-Sb-Cu),[22] $Pb_{0.9865}Ga_{0.0125}In_{0.001}S$ (PbS-Ga-In),[31] PbS-3%SrS-1%$PbCl_2$ (PbS-Sr-Cl),[21] PbS-1%Bi_2S_3-1%$PbCl_2$ (PbS-Bi-Cl),[20] p-type $Pb_{0.975}Na_{0.025}S$-3%CdS (PbS-Na-Cd (p)),[41] p-type $Pb_{0.975}Na_{0.025}S$-3%SrS (PbS-Na-Sr (p)),[19] and $Pb_{0.997}(GaSb)_{0.003}S$ (this work) samples.